# Pressure Balance between Solar Wind and Magnetosphere[1]

M. A. SCHIELD[2]

*Department of Space Science*
*Rice University, Houston, Texas 77001*

An evaluation of the subsolar pressure balance between the solar wind and the geomagnetic field shows that the average proton density of the quiet-day solar wind (300–400 km/sec) should be between 6 and 10 p/cm³. Even during storm times the proton density should always be between 2 p/cm³ and 70 p/cm³. The relation between the interplanetary solar-wind parameters and the stagnation pressure is reviewed. The subsolar geomagnetic field, including the quiet-day ring current field, is evaluated as a function of subsolar distance. The quiet-day ring current is based on the dipole gradient-drift motion of the low-energy protons observed by Davis and Williamson and by Frank. This quiet-day ring current has a magnetic moment of 0.26 $M_E$ and produces a 41-$\gamma$ decrease at the earth's surface. A geomagnetic field normalization of observed boundary distances is also proposed to remove the effects of the dipole tilt to the solar wind.

## INTRODUCTION

The size of the magnetosphere and the pressure of the solar wind are related by the pressure balance equation $p + B^2/2\mu_0 =$ constant. For a field-free solar wind and a plasma-free geomagnetic field this equation reduces to $p_0 = B_s^2/2\mu_0$. The subsolar solar-wind pressure $p_0$ was first calculated by assuming specular reflection of the noninteracting ions and electrons and was given by $p_0 = 2\rho v^2$ where $\rho$ is the mass density and $v$ is the solar wind velocity. The subsolar geomagnetic field $B_s$ was first assumed to be twice the tangential component of the subsolar dipole field in analogy with the confinement of a dipole field by a plane boundary. A self-consistent solution of the Chapman-Ferraro problem [*Mead and Beard*, 1964] indicated that the geomagnetic field was actually 2.44 times the dipole field at the subsolar point [*Mead*, 1964]. See *Beard* [1964] for a review. On these bases a 400-km/sec solar wind containing about 2.4 p/cm³ would confine the geomagnetic field to a subsolar distance of 11 $R_E$.

However, this conclusion is based on Chapman-Ferraro theory, which assumes that the solar plasma is noninteracting and field-free and assumes that the geomagnetic field is free of internal plasma. Observations of the solar wind [*Wilcox et al.*, 1967], of plasma energy densities within the magnetosphere [*Davis and Williamson*, 1963; *Frank*, 1967], and of the geomagnetic field [*Mead and Cahill*, 1967] indicate these assumptions are not satisfied. The purpose of this paper is to evaluate the pressure balance between the shocked solar wind and the magnetosphere with its internal plasma. The solar wind pressure necessary to confine the magnetosphere to a given subsolar distance is calculated. The proton number density of the solar wind is deduced from observations of the size of the magnetosphere and the velocity and composition of the solar wind and is compared with observations.

## SOLAR WIND PRESSURE

The body pressure $p_0$ of the shocked solar wind on the subsolar point of the magnetosphere may be related to the interplanetary solar wind momentum flux $\rho v^2$ at 1 AU by a solar wind pressure coefficient $K$ defined by $K = p_0/\rho v^2$. The value of $K$ depends upon the model of the solar wind. See *Spreiter et al.* [1966] for a review. In the steady-state condition the zero-temperature, field-free solar wind has a $K$ of 2 appropriate to an elastic collision. In the gas-dynamic approximation ($B = 0$) for a blunt-

[1] Based on thesis submitted in partial fulfillment of the requirements for the Ph.D. at Rice University.

[2] Present address: Physics Research Center, University of Iowa, Iowa City, Iowa 52240.

nosed obstacle in a hypersonic stream, $K$ is 0.844 for $\gamma = 2$ and 0.881 for $\gamma = 5/3$.

When the solar wind passes a magnetic field in aligned flow the stagnation pressure is given by $p_{max}^*/(\rho v^2) = 1 - (\frac{1}{2})\epsilon\,[1 + 2/((\gamma - 1)M^2)]$ where $\epsilon = (\gamma - 1)/(\gamma + 1)$ and $p^* = p + B^2/2\mu_0$ [*Lees*, 1964; *Hayes and Probstein*, 1959, p. 14]. For hypersonic flow ($M^2 \gg 1$) this relation reduces to 5/6 (0.832) for $\gamma = 2$ and to 7/8 (0.875) for $\gamma = 5/3$.

If the interplanetary field has a component perpendicular to the free stream velocity vector, the gasdynamic approximation breaks down at the stagnation point [*Alksne*, 1967]. When the interplanetary field is antiparallel to the subsolar geomagnetic field, the total stagnation pressure is $(2/3)\rho v^2$ for $\gamma = 2$ [*Lees*, 1964]. No coefficient is presently available for the parallel or perpendicular cases.

## Geomagnetic Field Pressure

The geomagnetic field is the sum of the earth's internal field, the magnetospheric surface-current field, and the field produced by plasmas within the magnetosphere of which the quiet-day and storm-time ring currents are examples. The ratio of the subsolar geomagnetic field $B_g$ to the subsolar dipole field $B_d$ is nearly independent of the subsolar distance in simple magnetospheric models and will be designated by $2f$ [*Ferraro*, 1960]. In an image dipole magnetosphere $f$ equals 1, while for a two-dimensional line dipole confined by a streaming plasma $f$ is less than 1 [*Chapman*, 1963]. In the Mead-Beard magnetosphere, which contains no internal plasma and no neutral sheet, $B_g/B_d$ equals 2.44 so that $f$ equals 1.22 [*Mead*, 1964].

The field of the quiet-day ring current is derived and discussed in the Appendix. This ring current is based on low-energy proton energy densities measured by *Davis and Williamson* [1963] and by *Frank* [1967]. These energy densities, illustrated in Figure 1, are

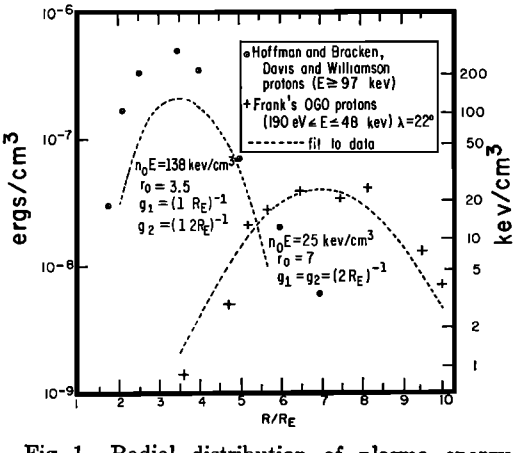


Fig. 1. Radial distribution of plasma energy densities observed by *Davis and Williamson* [1963] and by *Frank* [1967]. The parameters and the resultant functional forms used to describe these energy densities are also illustrated. Future observation of protons between 50 and 100 kev should fill in the gap in energy density around $L = 5$.

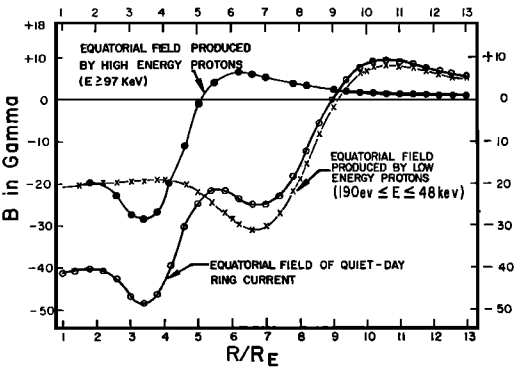


Fig. 2. Equatorial field of the quiet-day ring current obtained as the sum of the fields produced by the high- and low-energy components of the magnetospheric plasma. Inclusion of protons between 50 and 100 kev should smooth out the bump at $L = 5$.

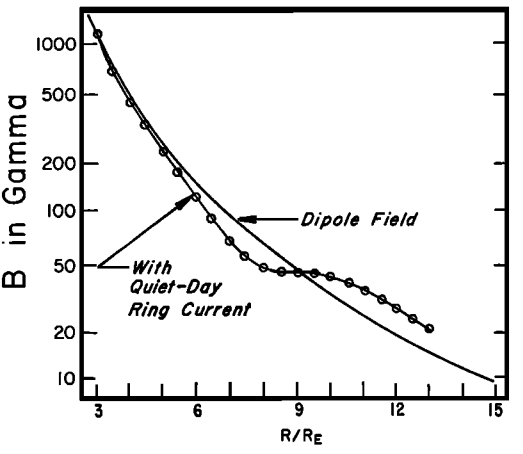


Fig. 3. Sum of the quiet-day ring current field and the earth's dipole field versus equatorial distance.

assumed to be symmetric and moving in a dipolar magnetic field. The equatorial quiet-day ring current field, illustrated in Figure 2, produces a 41-$\gamma$ decrease at the earth's surface and a maximum decrease of 58 $\gamma$ at 3.5 $R_E$. The equatorial ring-current field changes sign at 9 $R_E$ and enhances the dipole field by 8 to 10 $\gamma$ between 10 and 11.5 $R_E$. The sum of the dipole field and quiet-day ring current field is shown in Figure 3. This quiet-day ring current field is consistent with satellite observations [*Mead and Cahill*, 1967], illustrated in Figure 4. The net external field caused by the ring current and magnetopause currents is shown to be consistent with the external field statistically derived from ground-based observations [*Cain*, 1966]. The quiet-day ring current has a total magnetic moment of 0.26 $M_E$. Between 10 and 12 $R_E$, the ring current field enhances the equatorial dipole field by 25% to 35%, whereas along the polar axis, the dipole field is enhanced by 15% to 17% over the same radial region.

To calculate the subsolar geomagnetic field while including internal plasmas, the entire problem should be reworked self-consistently. However, the zeroth-order effect of this ring current field is to enhance the earth's dipole moment by 26% beyond 10 $R_E$. By neglecting

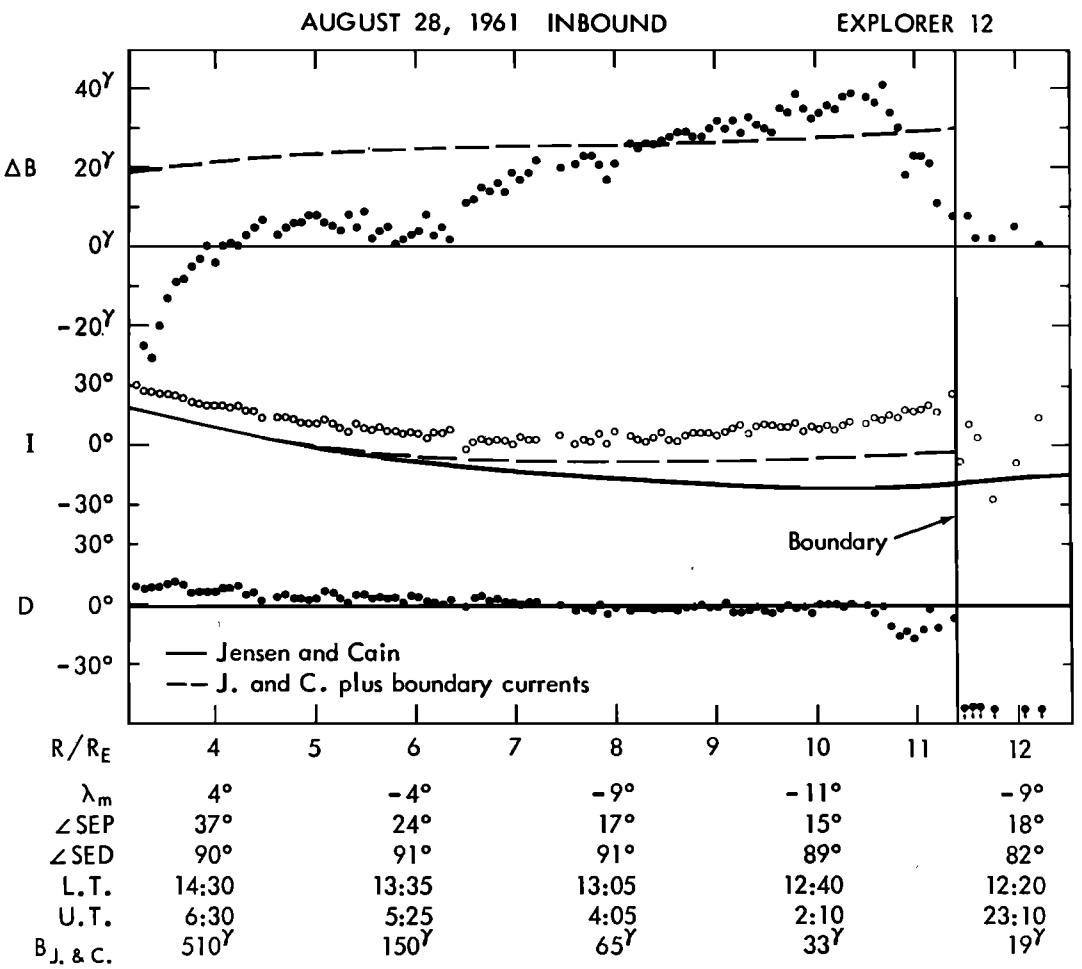


Fig. 4. Difference between the observed geomagnetic field within 30° of the subsolar axis for DST $\leq$ 10 $\gamma$ and the theoretically predicted geomagnetic field [*Mead*, 1964] assuming no internal plasma [*Mead and Cahill*, 1967]. The field of the quiet-day ring current (Figure 2) is capable of explaining this difference.

higher-order effects, the shape of the magnetosphere remains unchanged from that obtained by Mead and Beard. In this case, the subsolar geomagnetic field continues to be 2.44 times the internal field, which now includes both the dipole and ring current fields. The ratio $B_s/B_d$ is now 26% greater than 2.44 so that in the self-consistent magnetosphere with this quiet-day ring current field $f$ equals 1.54. Consideration of the nondipolar aspect of the ring current field would increase both the ring current field and the surface currents in the equatorial plane, thus increasing the subsolar geomagnetic field at the boundary.

*Normalization of subsolar boundary distances.* Since the subsolar geomagnetic field is also a function of subsolar latitude $\lambda_{ss}$, the subsolar boundary distances must be normalized to remove this variation. When the dipole axis is perpendicular to the solar wind the geomagnetic field pressure in the noon meridian plane is proportional to $\cos^3\lambda$ over the region where the magnetospheric boundary is circular [Figure 7; *Mead*, 1964]. This relation is based on the equality of the geomagnetic pressure and the solar wind pressure. If the subsolar geomagnetic field is assumed to be equal to the geomagnetic field at that same latitude for $\lambda_{ss} = 0°$, the normalization factor is $\cos^{-1/3}\lambda_{ss}$. This total-field normalization increases observed boundary distances by up to 7%.

The dipole normalization used by *Ness et al.* [1964] and by *Patel and Dessler* [1966] decreased boundary distances by up to 12%. Their normalization assumed the subsolar geomagnetic field was proportional to the total magnitude of the subsolar dipole field. The total-field normalization presented here is equivalent to assuming that the subsolar geomagnetic field is proportional to the angular component of the subsolar dipole field.

*Storm-time ring current field.* Beyond 7 $R_E$ the ratio between the storm-time ring-current field and the earth's dipole field may be described by $(-\text{DST}/700\ \gamma)$ in the equatorial plane. This ratio assumes the induction field produces a third of the total DST but no significant field beyond 7 $R_E$ [*Kavanagh*, 1967; 1968]. For a constant solar wind pressure a storm-time ring-current field with DST $\simeq -180$ $\gamma$ would increase the subsolar distance by about 8%, a DST of $-500$ $\gamma$ would increase the subsolar distance by about 20%. However, the disturbance field at the earth can be enhanced by up to a 100 $\gamma$ if the magnetopause expands from 6 to 10 $R_E$ [*Mead*, 1964].

Large subsolar distances often occur during the recovery phases of geomagnetic storms [*Freeman*, 1964]. Unless the storm is quite large (DST $\ll -180$ $\gamma$), it appears that a decrease in the solar wind pressure after the high-pressure geomagnetic storm condition must be the primary cause of these large subsolar distances rather than the internal pressure of the main-phase ring current.

*Tail current field.* The field produced by the tail currents forming the neutral sheet opposes the subsolar geomagnetic field. A split solenoid model of these tail currents is illustrated in Figure 5. The field a tail radius ahead of this configuration along the axis is 5% of the tail field. For tail fields of less than 30 $\gamma$ with an inner edge at 10 $R_E$, and a tail radius of 20 $R_E$ the subsolar tail current field is less than 1.5 $\gamma$. This southward-directed tail field is less than the northward-directed nondipolar component of the quiet-day ring current field and is, therefore, neglected.

Under the same conditions the truncated current sheet model [*Williams and Mead*, 1965] would produce a 22-$\gamma$ tail field at the subsolar point when the sheet has an outer edge of 200 $R_E$. However, this model is unsatisfactory because the current loop is completed entirely at infinity and not on the surface of the magnetosphere, giving the length of the geomagnetic

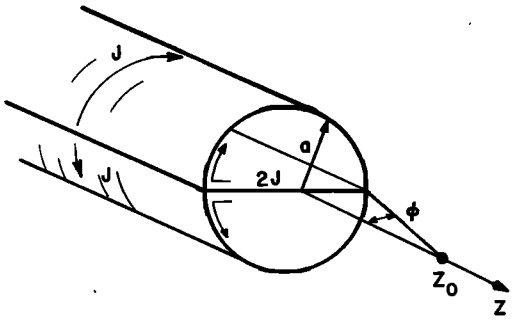


Fig. 5. Split solenoid model of the tail currents. The field measured on the axis ahead of this semi-infinite configuration is given by $B(z_0) = (\mu_0 J/2\pi)[\ln[(1 + \alpha)/(1 - \alpha)] - 2\alpha]$ where $\alpha = [1 + (z_0/a)^2]^{(-1/2)} = \sin\varphi$ (J. Midgley, personal communication).

TABLE 1. Solution of $n_1^* = [2B_0R_b^{-3}]^2/(2\mu_0 m_p v^2)$ Where $B_0 = 0.31$ Gauss

| Solar Wind Velocity, km/sec | Subsolar Distance in Earth Radii | | | | | | |
|---|---|---|---|---|---|---|---|
| | 12 | 11 | 10 | 9 | 8 | 7 | 6 |
| 300 | 3.40 | 5.74 | 10.2 | 19.1 | 38.8 | 86.4 | 218. |
| 400 | 1.91 | 3.23 | 5.72 | 10.8 | 21.8 | 48.6 | 123. |
| 500 | 1.23 | 2.06 | 3.66 | 6.88 | 14.0 | 31.1 | 78.4 |
| 600 | .85 | 1.43 | 2.54 | 4.78 | 9.69 | 21.6 | 54.4 |
| 700 | .63 | 1.05 | 1.87 | 3.51 | 7.12 | 15.9 | 40.0 |
| 800 | .48 | .81 | 1.43 | 2.69 | 5.45 | 12.1 | 30.6 |

tail an unrealistic influence on the subsolar tail field.

## Pressure Balance

The resultant pressure balance equation is given by

$$K\rho v^2 = (2fB_0R_b^{-3})^2/2\mu_0$$

where $K$ and $f$ are based on the models of the solar wind and geomagnetic field, respectively. $B_0$ is the equatorial dipole field and $R_b$ is the subsolar boundary distance. The assumption that the magnetopause is a tangential discontinuity appears to be valid most of the time [*Sonnerup and Cahill*, 1968]. The pressure of the plasmas just inside the magnetopause has been neglected although their presence will increase the solar wind pressure necessary to confine the geomagnetic field.

The mass density may be expressed in terms of an effective number density $n^*$ where $n^* = \rho/m_p$ [*Mead*, 1964]. For a neutral proton-electron gas, $n^*$ is the number density of each, neglecting $m_e/m_p$. Table 1 illustrates the required number density $n_1^*$ for the inelastic collision ($K = 1$) and image dipole ($f = 1$) models at selected subsolar distances and solar wind velocities.

The effective number densities for other values of $K$ and $f$ are related to $n_1^*$ by $n^* = (f^2/K)n_1^*$. Table 2 illustrates various values of the factor $(f^2/K)$ based on various models previously discussed. These results may be summarized by

$$n^*(\text{no./cm}^3)v^2(100\text{ km/sec})(R_b/10)^6 = 91.45(f^2/K)$$

## Observations and Discussions

The average solar wind velocity ranges from 300 to 800 km/sec but during quiet times is between 300 and 400 km/sec. See *Lüst* [1967] for a review of the properties of interplanetary space. The helium-hydrogen ratio varies between 0% and 15% and averages about 5%. The solar wind is normally hypersonic ($M^2 \gg 1$) since the thermal energy density $nkT$ is 1%–2% of the streaming energy density $\rho v^2$ and there is generally equipartition of energy

TABLE 2. Values of the Factor $(f^2/K)$ for Various Models

| $K = p_0/(pv^2)$ | | | $f = B_e/2B_d$ | | |
|---|---|---|---|---|---|
| | | | Image Dipole 1.00 | Self-Consistent Dipole 1.22 | Self-Consistent Dipole and Ring Current 1.54 |
| 1.000 | inelastic collision | | 1.00 | 1.49 | 2.36 |
| 0.881 | gasdynamic | $\gamma = 5/3$ | 1.14 | 1.69 | 2.68 |
| 0.875 | aligned flow | $\gamma = 5/3$ | 1.14 | 1.70 | 2.70 |
| 0.844 | gasdynamic | $\gamma = 2$ | 1.18 | 1.76 | 2.80 |
| 0.832 | aligned flow | $\gamma = 2$ | 1.20 | 1.79 | 2.84 |
| 0.667 | antiparallel | $\gamma = 2$ | 1.50 | 2.23 | 3.54 |

between the thermal energy density and the magnetic field energy density.

The measurements of the proton density in the quiet-time solar wind appear to fall into two groups depending on the type of instrument utilized. The curved-plate analyzer measurements (Mariner 2 and 4, Wolfe on IMP 1 and 2, and Pioneer 6, Vela 2 and 3) indicate the quiet-time solar wind proton density is between 1 and 5 p/cm$^3$. The Faraday cup measurements (Bridge on IMP 1, Mariner 4, and Pioneer 6) indicate the proton density of the quiet-time solar wind is between 5 and 10 p/cm$^3$ [*Wilcox et al.*, 1967; *Lazarus et al.*, 1966].

The subsolar extent of the magnetopshere has been analyzed by *Ness et al.* [1964] and by *Patel and Dessler* [1966]. Both used the dipole normalization discussed previously. A subsolar radius of 10.25 $R_E$ provided the best fit of the IMP 1 data to the theoretical shape of the magnetosphere. For 60 boundary crossings within 75° of the subsolar point, Patel and Dessler deduced subsolar radii between 6.9 and 11.5 $R_E$. Since all of these observations were made during the winter, the use of the total field normalization would increase these values by up to 20%. On this basis, the average subsolar distance is expected to be between 10.5 and 11 $R_E$.

If the number density ratio of helium to hydrogen is taken as 10%, the proton number density is 71.5% of the effective number density since $n_p = n^*/(1 + 4\ n_\alpha/n_p)$. On the basis of the pressure balance relation, this 400-km/sec solar wind must have between 6.2 p/cm$^3$ and 8.2 p/cm$^3$ to contain the geomagnetic field to a subsolar distance of 11 $R_E$, and have between 11.0 p/cm$^3$ and 14.5 p/cm$^3$ for a subsolar distance of 10 $R_E$.

Although these values are in direct disagreement with some curved-plate analyzer observations, they are in agreement with the MIT plasma cup measurements [*Lazarus et al.*, 1966] and with group path measurements [*Eshleman and others*, 1966]. Using Pioneer 6 the problem of correcting for ionospheric electrons was solved by utilizing a source that is continuously moving away from the earth. Near the earth's oribt the average interplanetary electron number density was determined to be between 8 and 9 e/cm$^3$ with an rms deviation of 4.4 e/cm$^3$.

It is, therefore, concluded that the quiet-day solar wind (350–400 km/sec) has an average proton density of about 6 to 10 p/cm$^3$. Furthermore, the proton density must always be greater than 2 p/cm$^3$ unless the solar wind velocity exceeds 800 km/sec and the subsolar radius simultaneously exceeds 11 $R_E$. The proton density should always be less than 70 p/cm$^3$ unless the subsolar radius is less than 6 $R_E$ while the solar wind velocity is less than 800 km/sec.

## Appendix. The Quiet-Day Ring Current

*Plasma energy densities and currents.* The radial distribution of plasmas having sufficient energy density to contribute significantly to the quiet-day ring current are illustrated in Figure 1. *Hoffman and Bracken* [1965] noted that, owing to a recalibration of the detectors, the Davis and Williamson fluxes and, therefore, their energy densities, should be increased by 25%. However, *Davis and Williamson* [1966] observed that the flux has a variation of 25% and that particles below 300 kev have decreased by 25% between 1961 and 1965. Therefore, the energy densities deduced by Hoffman and Bracken have been utilized as originally presented. Frank's data were taken at a geomagnetic latitude of 22° ± 2° and for $5 \leq L \leq 11$ were taken within 15° of the dusk meridian.

The analysis of the ring currents produced by plasmas in the dipole field is simplified when the equatorial energy density is fit to the form $NE = (N_0E)\exp\{-[g_i\ (L - r_0)]^2\}$ where $i$ equals 1 for $L \leq r_0$ and i equals 2 for $L \geq r_0$ (see *Akasofu and Chapman* [1967] and references therein). A flux distribution of the form $f(B, \varphi) = \sin^\alpha \varphi B^{-\alpha/2}$, where $\varphi$ is the pitch angle, has proven to be both convenient and realistic in fitting particle distribution. Thus in this model the five parameters $N_0E$, $r_0$, $\alpha$, $g_1$, and $g_2$ completely specify the ring current and its associated field.

Hoffman and Bracken determined that the values $N_0E = 138$ kev/cm$^3$, $r_0 = 3.5$, $\alpha = 2.5$, $g_1 = (1\ R_E)^{-1}$, $g_2 = (1.25\ R_E)^{-1}$ provided a 'best fit' to plasmas above 100 kev. They also found that in this energy range $\alpha$ decreased with decreasing energy and with increasing distance. Frank's data has been fit by the parameters $r_0 = 7$, and $g_1 = g_2(2\ R_E)^{-1}$. A knowledge of the pitch-angle distribution is necessary to obtain the equatorial energy density from that measured along the same field line at higher latitudes. Detailed pitch-angle information is not yet

available, but it is likely that $\alpha$ lies between 0 and 2. It has been assumed somewhat arbitrarily that the maximum equatorial energy density $N_0E$ is 25 kev/cm$^3$ and that $\alpha$ equals 2. Since this choice reflects the minimum equatorial energy ($\alpha = 0$) and limits the particle distribution to low latitudes ($\alpha = 2$), future data may enhance the total energy of the quiet-day ring current. Figure 1 also illustrates the values of these functions versus $L$.

The derivation of the ring current field is based on the integration over the resultant current density [*Kavanagh*, 1968; Appendix A]. A computer calculation, prepared by Dr. Kavanagh, which assumes that all particles are confined to a region bounded by the earth's surface and the dipole shell with $L = 10$ has been used to determine the ring current field.

*Properties of the ring current field.* The fields due to these ring currents are illustrated in Tables 3–6. The field of the quiet-day ring current is the sum of these fields. The equatorial fields of these ring currents are shown in Figure 2. The sum of the earth's dipole field and the

TABLE 3

Values of the theta component of the magnetic field in gammas produced by a ring current band of charged particles described by the parameters: $N_0E = 25$ kev/cm$^3$, $R_0 = 7.0$, $g_1 = g_2 = (2\ R_E)^{-1}$, $\alpha = 2.0$. Negative values denote opposed in sense to geomagnetic field. By symmetry the theta component is zero at 90° latitude.

| Geocentric Distance, $R_E$ | Latitude, deg | | | | | | | | |
|---|---|---|---|---|---|---|---|---|---|
| | 80 | 70 | 60 | 50 | 40 | 30 | 20 | 10 | 0 |
| 1.0 | −3.7 | −7.2 | −10.5 | −13.4 | −15.9 | −18.0 | −19.4 | −20.3 | −20.6 |
| 1.4 | −3.7 | −7.3 | −10.6 | −13.5 | −16.0 | −18.0 | −19.4 | −20.2 | −20.5 |
| 1.8 | −3.7 | −7.3 | −10.7 | −13.7 | −16.1 | −18.0 | −19.3 | −20.1 | −20.3 |
| 2.2 | −3.7 | −7.3 | −10.8 | −13.9 | −16.4 | −18.2 | −19.3 | −19.9 | −20.1 |
| 2.6 | −3.6 | −7.3 | −10.9 | −14.3 | −16.8 | −18.3 | −19.3 | −19.7 | −19.9 |
| 3.0 | −3.5 | −7.1 | −10.9 | −14.8 | −17.4 | −18.5 | −19.3 | −19.5 | −19.6 |
| 3.4 | −3.2 | −6.7 | −10.5 | −15.0 | −18.0 | −18.8 | −19.5 | −19.4 | −19.4 |
| 3.8 | −2.9 | −6.1 | −9.8 | −14.5 | −18.0 | −19.4 | −20.1 | −19.4 | −19.3 |
| 4.2 | −2.6 | −5.5 | −8.9 | −13.2 | −17.5 | −20.6 | −21.3 | −19.6 | −19.5 |
| 4.6 | −2.3 | −4.8 | −7.8 | −11.5 | −16.8 | −22.3 | −23.0 | −20.3 | −20.4 |
| 5.0 | −2.0 | −4.2 | −6.9 | −10.1 | −16.1 | −24.3 | −25.0 | −21.7 | −22.1 |
| 5.4 | −1.7 | −3.6 | −5.9 | −9.1 | −15.4 | −25.4 | −26.5 | −23.9 | −24.6 |
| 5.8 | −1.4 | −3.1 | −5.1 | −8.1 | −14.0 | −24.8 | −26.9 | −26.6 | −27.5 |
| 6.2 | −1.2 | −2.5 | −4.2 | −6.8 | −11.9 | −21.8 | −25.6 | −29.2 | −30.0 |
| 6.6 | −1.0 | −2.1 | −3.5 | −5.5 | −9.3 | −16.9 | −22.8 | −30.9 | −31.2 |
| 7.0 | −0.8 | −1.7 | −2.8 | −4.3 | −6.7 | −11.1 | −18.7 | −30.7 | −30.4 |
| 7.4 | −0.6 | −1.3 | −2.1 | −3.2 | −4.4 | −5.6 | −14.1 | −28.0 | −27.2 |
| 7.8 | −0.5 | −1.0 | −1.6 | −2.2 | −2.5 | −1.6 | −9.6 | −22.8 | −21.9 |
| 8.2 | −0.4 | −0.8 | −1.2 | −1.5 | −1.2 | 0.6 | −5.6 | −15.7 | −15.2 |
| 8.6 | −0.3 | −0.6 | −0.8 | −0.9 | −0.3 | 1.5 | −2.3 | −8.0 | −8.2 |
| 9.0 | −0.2 | −0.4 | −0.5 | −0.4 | 0.3 | 1.8 | 0.4 | −0.7 | −1.9 |
| 9.4 | −0.1 | −0.3 | −0.3 | −0.1 | 0.7 | 2.0 | 2.4 | 4.8 | 2.9 |
| 9.8 | −0.1 | −0.1 | −0.1 | 0.2 | 0.9 | 2.2 | 3.7 | 8.0 | 6.1 |
| 10.2 | 0.0 | −0.1 | 0.1 | 0.4 | 1.1 | 2.3 | 4.4 | 9.0 | 7.6 |
| 10.6 | 0.0 | 0.0 | 0.2 | 0.5 | 1.2 | 2.4 | 4.6 | 8.7 | 8.0 |
| 11.0 | 0.0 | 0.1 | 0.2 | 0.6 | 1.3 | 2.4 | 4.5 | 7.9 | 7.7 |
| 11.4 | 0.0 | 0.1 | 0.3 | 0.7 | 1.3 | 2.4 | 4.3 | 7.0 | 7.1 |
| 11.8 | 0.1 | 0.2 | 0.4 | 0.7 | 1.3 | 2.3 | 4.0 | 6.2 | 6.4 |
| 12.2 | 0.1 | 0.2 | 0.4 | 0.7 | 1.3 | 2.2 | 3.7 | 5.4 | 5.8 |
| 12.6 | 0.1 | 0.2 | 0.4 | 0.7 | 1.3 | 2.1 | 3.4 | 4.8 | 5.2 |
| 13.0 | 0.1 | 0.2 | 0.4 | 0.7 | 1.2 | 2.0 | 3.1 | 4.3 | 4.6 |

TABLE 4

Values of the radial component of the magnetic field in gammas produced by a ring current band of charged particles described by the parameters: $N_0E = 25$ kev/cm$^3$, $R_0 = 7.0$, $g_1 = g_2 = (2\ R_E)^{-1}$, $\alpha = 2.0$. Negative values denote opposed in sense to geomagnetic field. By symmetry the radial component is zero at 0° latitude.

| Geocentric Distance, $R_E$ | Latitude, deg | | | | | | | | |
|---|---|---|---|---|---|---|---|---|---|
| | 90 | 80 | 70 | 60 | 50 | 40 | 30 | 20 | 10 |
| 1.0 | 23.3 | 20.6 | 19.6 | 18.0 | 15.9 | 13.3 | 10.3 | 7.0 | 3.5 |
| 1.4 | 22.8 | 20.7 | 19.7 | 18.0 | 15.9 | 13.2 | 10.2 | 6.9 | 3.5 |
| 1.8 | 22.5 | 20.8 | 19.9 | 18.1 | 15.9 | 13.2 | 10.1 | 6.8 | 3.4 |
| 2.2 | 22.3 | 20.9 | 20.0 | 18.3 | 15.9 | 13.1 | 9.9 | 6.6 | 3.3 |
| 2.6 | 22.1 | 20.9 | 20.1 | 18.6 | 16.1 | 13.1 | 9.6 | 6.4 | 3.1 |
| 3.0 | 21.7 | 20.8 | 20.2 | 19.0 | 16.6 | 12.9 | 9.3 | 6.1 | 2.9 |
| 3.4 | 21.2 | 20.4 | 20.1 | 19.4 | 17.6 | 12.5 | 8.9 | 5.8 | 2.6 |
| 3.8 | 20.5 | 19.9 | 19.9 | 19.7 | 18.7 | 12.3 | 8.7 | 5.5 | 2.2 |
| 4.2 | 19.7 | 19.2 | 19.4 | 19.7 | 19.5 | 12.8 | 8.9 | 4.9 | 1.6 |
| 4.6 | 18.7 | 18.4 | 18.7 | 19.3 | 19.6 | 14.2 | 9.8 | 4.1 | 1.0 |
| 5.0 | 17.7 | 17.5 | 17.9 | 18.7 | 19.3 | 16.4 | 11.6 | 2.9 | 0.4 |
| 5.4 | 16.7 | 16.5 | 17.0 | 17.9 | 18.9 | 18.5 | 14.0 | 1.8 | 0.1 |
| 5.8 | 15.7 | 15.5 | 16.1 | 17.1 | 18.6 | 20.2 | 16.7 | 1.2 | 0.4 |
| 6.2 | 14.7 | 14.5 | 15.2 | 16.3 | 18.1 | 21.2 | 19.2 | 1.6 | 1.3 |
| 6.6 | 13.7 | 13.6 | 14.2 | 15.4 | 17.4 | 21.4 | 20.8 | 3.3 | 2.9 |
| 7.0 | 12.7 | 12.6 | 13.2 | 14.4 | 16.5 | 20.7 | 21.3 | 6.1 | 4.9 |
| 7.4 | 11.8 | 11.7 | 12.3 | 13.4 | 15.5 | 19.4 | 20.6 | 9.5 | 6.9 |
| 7.8 | 11.0 | 10.9 | 11.4 | 12.5 | 14.3 | 17.7 | 19.0 | 12.7 | 8.5 |
| 8.2 | 10.2 | 10.1 | 10.6 | 11.5 | 13.2 | 15.9 | 17.1 | 14.9 | 9.6 |
| 8.6 | 9.4 | 9.4 | 9.8 | 10.6 | 12.0 | 14.2 | 15.3 | 15.8 | 10.0 |
| 9.0 | 8.7 | 8.7 | 9.1 | 9.8 | 11.0 | 12.7 | 13.7 | 15.5 | 9.6 |
| 9.4 | 8.1 | 8.0 | 8.4 | 9.0 | 10.0 | 11.3 | 12.3 | 14.4 | 8.8 |
| 9.8 | 7.5 | 7.4 | 7.7 | 8.3 | 9.1 | 10.1 | 11.0 | 12.7 | 7.7 |
| 10.2 | 7.0 | 6.9 | 7.1 | 7.6 | 8.3 | 9.1 | 9.8 | 11.0 | 6.5 |
| 10.6 | 6.5 | 6.4 | 6.6 | 7.0 | 7.5 | 8.2 | 8.7 | 9.4 | 5.5 |
| 11.0 | 6.0 | 5.9 | 6.1 | 6.4 | 6.9 | 7.4 | 7.8 | 8.0 | 4.7 |
| 11.4 | 5.6 | 5.5 | 5.7 | 5.9 | 6.3 | 6.7 | 6.9 | 6.8 | 4.0 |
| 11.8 | 5.2 | 5.1 | 5.2 | 5.5 | 5.8 | 6.0 | 6.2 | 5.8 | 3.4 |
| 12.2 | 4.8 | 4.8 | 4.9 | 5.1 | 5.3 | 5.5 | 5.5 | 5.0 | 2.9 |
| 12.6 | 4.5 | 4.4 | 4.5 | 4.7 | 4.8 | 5.0 | 4.9 | 4.4 | 2.5 |
| 13.0 | 4.2 | 4.1 | 4.2 | 4.3 | 4.4 | 4.5 | 4.4 | 3.8 | 2.2 |

quiet-day ring current field in the equatorial plane is shown in Figure 3. It is interesting to note that this first-order calculation may be rather self-consistent in the sense that the gradient of the total field never changes sign.

The magnetic moment of this quiet-day ring current is 0.26 $M_E$, based on the value of the ring current field at large distances (50–130 $R_E$). The low-energy particles ($E \leq 50$ kev) being located at twice the radius of the higher energy particles produce about 85% of this magnetic moment. This 26% increase in the earth's magnetic moment could have considerable effect on cosmic-ray observations except for the nearness of the outer ring current belt to the magnetospheric boundary.

The total energy of this quiet-day ring current is $12.7 \times 10^{23}$ ergs, 58% of which is contained by the lower energy protons ($E \leq 50$ kev). The difference between the 33.5-$\gamma$ field predicted by *Sckopke's* [1966] first-order relation and the 41-$\gamma$ field obtained by integrating over the currents could be reduced by including the field energy of the ring current.

*Comparison with observations.* Magnetic observations by Explorer 12 indicated that there were two deficiencies in the *Mead* [1964] model of the geomagnetic field [*Mead and Cahill*, 1967]. First, the inclusion of a neutral-sheet tail field would probably explain the enhanced twisting and expansion of field lines along the flanks of the magnetosphere. Second, the field of the quiet-day ring current (Figure 2) would explain the observed deviations from Mead's model illustrated in Figure 4. This conclusion is not significantly altered by the 26% increase (4–7 $\gamma$) in the surface current field due to the presence of these internal plasmas.

Based on the analysis of terrestrial magnetic data *Cain* [1966] determined the existence of a statistically significant external field of 26.41 $\gamma$. The component of this field parallel to the dipole axis is 20.8 $\gamma$ and is directed southward. The 41-$\gamma$ southward-directed field of the quiet-day ring current is necessary to explain these surface observations. The field of the surface currents is directed northward and is about 26 $\gamma$, when enhanced by 26%, for a subsolar

TABLE 5

Values of the theta component of the magnetic field in gammas produced by a ring current band of charged particles described by the parameters: $N_0E_0 = 138$ kev/cm$^3$, $R_0 = 3.5$, $g_1 = (1\,R_E)^{-1}$, $g_2 = (1.2\,R_E)^{-1}$ $\alpha = 2.5$. Negative values denote opposed in sense to geomagnetic field. By symmetry the theta component is zero at 90° latitude.

| Geocentric Distance, $R_E$ | Latitude, deg | | | | | | | | |
|---|---|---|---|---|---|---|---|---|---|
| | 80 | 70 | 60 | 50 | 40 | 30 | 20 | 10 | 0 |
| 1.0 | −3.6 | −7.2 | −10.5 | −13.6 | −16.1 | −18.1 | −19.5 | −20.3 | −20.6 |
| 1.4 | −3.5 | −7.0 | −10.5 | −13.8 | −16.5 | −18.3 | −19.5 | −20.1 | −20.3 |
| 1.8 | −3.1 | −6.4 | −9.9 | −13.9 | −17.0 | −18.9 | −19.9 | −19.9 | −20.0 |
| 2.2 | −2.6 | −5.5 | −8.7 | −12.7 | −16.9 | −20.4 | −21.4 | −20.3 | −20.4 |
| 2.6 | −2.1 | −4.4 | −7.2 | −10.7 | −15.9 | −22.5 | −23.9 | −22.3 | −22.9 |
| 3.0 | −1.6 | −3.4 | −5.6 | −8.6 | −13.8 | −22.0 | −25.0 | −26.2 | −26.9 |
| 3.4 | −1.2 | −2.5 | −4.1 | −6.4 | −10.5 | −17.6 | −22.8 | −28.8 | −29.3 |
| 3.8 | −0.8 | −1.8 | −2.9 | −4.4 | −6.8 | −10.9 | −17.5 | −27.0 | −27.1 |
| 4.2 | −0.6 | −1.2 | −1.9 | −2.7 | −3.7 | −5.0 | −11.0 | −20.2 | −20.1 |
| 4.6 | −0.4 | −0.8 | −1.1 | −1.5 | −1.6 | −1.3 | −5.0 | −10.6 | −10.9 |
| 5.0 | −0.2 | −0.4 | −0.6 | −0.7 | −0.3 | 0.6 | −0.6 | −1.9 | −2.6 |
| 5.4 | −0.1 | −0.2 | −0.2 | −0.1 | 0.4 | 1.5 | 2.1 | 3.8 | 2.9 |
| 5.8 | 0.0 | −0.1 | 0.0 | 0.2 | 0.8 | 1.9 | 3.4 | 6.2 | 5.6 |
| 6.2 | 0.0 | 0.1 | 0.2 | 0.5 | 1.0 | 2.0 | 3.7 | 6.5 | 6.2 |
| 6.6 | 0.0 | 0.1 | 0.3 | 0.6 | 1.1 | 2.0 | 3.6 | 5.8 | 5.8 |
| 7.0 | 0.1 | 0.2 | 0.3 | 0.6 | 1.1 | 1.9 | 3.2 | 4.9 | 5.1 |
| 7.4 | 0.1 | 0.2 | 0.4 | 0.6 | 1.1 | 1.8 | 2.9 | 4.0 | 4.3 |
| 7.8 | 0.1 | 0.2 | 0.4 | 0.6 | 1.0 | 1.6 | 2.5 | 3.3 | 3.6 |
| 8.2 | 0.1 | 0.2 | 0.4 | 0.6 | 1.0 | 1.5 | 2.2 | 2.8 | 3.0 |
| 8.6 | 0.1 | 0.2 | 0.4 | 0.6 | 0.9 | 1.3 | 1.9 | 2.4 | 2.5 |
| 9.0 | 0.1 | 0.2 | 0.4 | 0.6 | 0.8 | 1.2 | 1.6 | 2.0 | 2.1 |
| 9.4 | 0.1 | 0.2 | 0.3 | 0.5 | 0.8 | 1.1 | 1.4 | 1.7 | 1.8 |
| 9.8 | 0.1 | 0.2 | 0.3 | 0.5 | 0.7 | 1.0 | 1.3 | 1.5 | 1.6 |
| 10.2 | 0.1 | 0.2 | 0.3 | 0.5 | 0.6 | 0.8 | 1.1 | 1.3 | 1.4 |
| 10.6 | 0.1 | 0.2 | 0.3 | 0.4 | 0.6 | 0.8 | 1.0 | 1.2 | 1.2 |
| 11.0 | 0.1 | 0.2 | 0.3 | 0.4 | 0.5 | 0.7 | 0.9 | 1.0 | 1.1 |
| 11.4 | 0.1 | 0.2 | 0.2 | 0.4 | 0.5 | 0.6 | 0.8 | 0.9 | 0.9 |
| 11.8 | 0.1 | 0.1 | 0.2 | 0.3 | 0.5 | 0.6 | 0.7 | 0.8 | 0.8 |
| 12.2 | 0.1 | 0.1 | 0.2 | 0.3 | 0.4 | 0.5 | 0.6 | 0.7 | 0.8 |
| 12.6 | 0.1 | 0.1 | 0.2 | 0.3 | 0.4 | 0.5 | 0.6 | 0.7 | 0.7 |
| 13.0 | 0.1 | 0.1 | 0.2 | 0.3 | 0.4 | 0.4 | 0.5 | 0.6 | 0.6 |

TABLE 6

Values of the radial component of the magnetic field in gammas produced by a ring current band of of charged particles described by the parameters: $N_0E$ = 138 kev/cm$^3$, $R_0$ = 3.5, $g_1 = (1\ R_E)^{-1}$, $g_2 = (1.2\ R_E)^{-1}$, $\alpha$ = 2.5. Negative values denote opposed in sense to geomagnetic field. By symmetry the radial component is zero at 0° latitude.

| Geocentric Distance, $R_E$ | Latitude, deg | | | | | | | | |
|---|---|---|---|---|---|---|---|---|---|
| | 90 | 80 | 70 | 60 | 50 | 40 | 30 | 20 | 10 |
| 1.0 | 22.2 | 20.6 | 19.7 | 18.1 | 16.0 | 13.3 | 10.2 | 6.9 | 3.5 |
| 1.4 | 21.6 | 20.4 | 19.7 | 18.4 | 16.3 | 13.3 | 10.0 | 6.7 | 3.3 |
| 1.8 | 20.6 | 19.8 | 19.5 | 18.8 | 17.2 | 13.3 | 9.7 | 6.2 | 2.9 |
| 2.2 | 19.3 | 18.7 | 18.8 | 18.8 | 18.2 | 14.1 | 10.2 | 5.4 | 2.1 |
| 2.6 | 17.6 | 17.3 | 17.6 | 18.1 | 18.5 | 16.3 | 12.3 | 4.2 | 1.4 |
| 3.0 | 15.9 | 15.6 | 16.1 | 17.0 | 18.1 | 18.6 | 15.6 | 3.8 | 1.8 |
| 3.4 | 14.1 | 13.9 | 14.5 | 15.5 | 17.2 | 19.7 | 18.4 | 5.7 | 3.7 |
| 3.8 | 12.4 | 12.3 | 12.9 | 13.9 | 15.7 | 18.9 | 19.3 | 9.4 | 6.4 |
| 4.2 | 10.9 | 10.8 | 11.3 | 12.3 | 14.0 | 16.9 | 18.1 | 13.0 | 8.5 |
| 4.6 | 9.5 | 9.5 | 9.9 | 10.7 | 12.1 | 14.5 | 15.9 | 14.7 | 9.4 |
| 5.0 | 8.3 | 8.3 | 8.6 | 9.3 | 10.4 | 12.1 | 13.4 | 14.3 | 8.9 |
| 5.4 | 7.3 | 7.2 | 7.5 | 8.0 | 8.9 | 10.0 | 11.1 | 12.4 | 7.6 |
| 5.8 | 6.4 | 6.3 | 6.5 | 7.0 | 7.6 | 8.4 | 9.1 | 10.0 | 6.1 |
| 6.2 | 5.6 | 5.5 | 5.7 | 6.0 | 6.5 | 7.0 | 7.5 | 7.8 | 4.7 |
| 6.6 | 4.9 | 4.9 | 5.0 | 5.2 | 5.5 | 5.9 | 6.1 | 6.0 | 3.6 |
| 7.0 | 4.4 | 4.3 | 4.4 | 4.5 | 4.8 | 4.9 | 5.0 | 4.7 | 2.8 |
| 7.4 | 3.9 | 3.8 | 3.9 | 4.0 | 4.1 | 4.2 | 4.2 | 3.7 | 2.2 |
| 7.8 | 3.4 | 3.4 | 3.4 | 3.5 | 3.6 | 3.6 | 3.5 | 3.0 | 1.7 |
| 8.2 | 3.1 | 3.0 | 3.0 | 3.1 | 3.1 | 3.1 | 2.9 | 2.4 | 1.4 |
| 8.6 | 2.7 | 2.7 | 2.7 | 2.7 | 2.7 | 2.7 | 2.5 | 2.0 | 1.1 |
| 9.0 | 2.4 | 2.4 | 2.4 | 2.4 | 2.4 | 2.3 | 2.1 | 1.7 | 0.9 |
| 9.4 | 2.2 | 2.1 | 2.1 | 2.1 | 2.1 | 2.0 | 1.8 | 1.4 | 0.8 |
| 9.8 | 2.0 | 1.9 | 1.9 | 1.9 | 1.9 | 1.8 | 1.6 | 1.2 | 0.7 |
| 10.2 | 1.8 | 1.7 | 1.7 | 1.7 | 1.7 | 1.6 | 1.4 | 1.1 | 0.6 |
| 10.6 | 1.6 | 1.6 | 1.6 | 1.5 | 1.5 | 1.4 | 1.2 | 0.9 | 0.5 |
| 11.0 | 1.5 | 1.4 | 1.4 | 1.4 | 1.3 | 1.2 | 1.1 | 0.8 | 0.4 |
| 11.4 | 1.4 | 1.3 | 1.3 | 1.3 | 1.2 | 1.1 | 1.0 | 0.7 | 0.4 |
| 11.8 | 1.2 | 1.2 | 1.2 | 1.1 | 1.1 | 1.0 | 0.8 | 0.6 | 0.3 |
| 12.2 | 1.1 | 1.1 | 1.1 | 1.0 | 1.0 | 0.9 | 0.8 | 0.6 | 0.3 |
| 12.6 | 1.0 | 1.0 | 1.0 | 1.0 | 0.9 | 0.8 | 0.7 | 0.5 | 0.3 |
| 13.0 | 1.0 | 0.9 | 0.9 | 0.9 | 0.8 | 0.7 | 0.6 | 0.5 | 0.2 |

distance of 11 $R_E$. The field of the split solenoid tail field model, measured half a tail radius ahead of the configuration, is about a sixth of the field within the geomagnetic tail and is directed southward. For an 18-$\gamma$ tail field the predicted external field at the earth is 18 $\gamma$ and is directed southward in excellent agreement with Cain's observations.

*Analysis of premises.* A self-consistent solution of the geomagnetic field including this quiet-day ring current field, to which a realistic tail field has been joined, indicates the geomagnetic field is nearly dipolar in both magnitude and configuration for $L \leq 7$ on the dayside and for $L \leq 6$ on the nightside *Schield* [1968]. Beyond these distances the geomagnetic field will enhance the nightside ring current while decreasing the dayside ring current relative to the current based on a dipole field configuration. No compensation for these effects has been made in view of the conservative evaluation of the maximum equatorial energy density of the low-energy particles forming the outermost portion of the ring current.

Although the exact configuration of the magnetospheric electric field is unknown, estimates of its magnitude are all below a mv/m in the equatorial plane. A 1-mv/m field would balance the gradient drift of particles below 15 kev beyond 7 $R_E$ of the earth. Since at least half of the energy density at $L = 6.0$ is carried by protons above 30 kev [*Frank*, 1967; Figure 11], the electric field may be considered a perturbation, albeit a very large perturbation. It does not seem reasonable, however, to evaluate the quiet-day ring current and field in any greater detail [*Hoffman and Bracken*, 1967] until the energy density distributions are known for various local times and the configuration and magnitude of the electric field are more adequately defined.

*Acknowledgments.* The author is indebted to Dr. A. J. Dessler for suggesting this problem and for commenting on this manuscript. The author would like to thank Dr. L. Kavanagh for the use of his ring current program and Dr. J. Midgley for providing the exact solution of the split-solenoid tail field along the axis of symmetry.

This work was supported in part by the U. S. Air Force Cambridge Research Laboratories under contract AF19(628)-3858.

## References

Akasofu, S.-I., and S. Chapman, Corrections to papers concerning magnetic effects of model ring currents, *J. Geophys. Res., 72,* 445, 1967.

Alksne, A. Y., The steady-state magnetic field in the transition region between the magnetosphere and the bow shock, *Planetary Space Sci., 15,* 239, 1967.

Beard, D. B., The solar wind geomagnetic field boundary, *Rev. Geophys., 2,* 335, 1964.

Cain, J. C., Models of the earth's magnetic field, in *Radiation Trapped in the Earth's Magnetic Field,* edited by Billy M. McCormac, p. 7, D. Reidel Publishing Company, Dordrecht-Holland, 1966.

Chapman, S., Solar plasma, geomagnetism and aurora, in *Geophysics, the Earth's Environment Les Houches Lectures 1962,* edited by DeWitt, Hieblot, and Lebeau, p. 373, *Gordon and Breach Publishers,* New York, 1963.

Davis, L. R., and J. M. Williamson, Low energy trapped protons, *Space Res., 3,* 365, 1963.

Davis, L. R., and J. M. Williamson, Outer zone protons in *Radiation Trapped in the Earth's Magnetic Field,* edited by Billy M. McCormac, p. 215, D. Reidel Publishing Co., Dordrecht-Holland, 1966.

Eshleman, V. R., and others, The interplanetary electron number density from preliminary analysis of the Pioneer 6 radio propagation experiment, *J. Geophys. Res., 71,* 3325, 1966.

Ferraro, V. C. A., An approximate method of estimating the size and shape of the stationary hollow carved out in a neutral ionized stream of corpuscles impinging on the geomagnetic field, *J. Geophys. Res., 65,* 3951, 1960.

Frank, L. A., Several observations of low-energy protons and electrons in the earth's magnetosphere with OGO 3, *J. Geophys. Res., 72,* 1905, 1967.

Freeman, J. W., Jr., The morphology of the electron distribution in the outer radiation zone and near the magnetospheric boundary as observed by Explorer 12, *J. Geophys. Res., 69,* 1691, 1964.

Hayes, W. D., and R. F. Probstein, *Hypersonic Flow Theory,* Academic Press, New York, 1959.

Hoffman, R. A., and P. A. Bracken, Magnetic effects of the quiet time proton belt, *J. Geophys. Res., 70,* 3541, 1965.

Hoffman, R. A., and P. A. Bracken, Higher-order ring currents and particle energy storage in the magnetosphere, *J. Geophys. Res, 72,* 6039, 1967.

Kavanagh, L. D., Jr., Predicted and observed displacements and energy changes of charged particles after distention of the magnetosphere by a symmetric ring current, Ph.D. thesis, Rice University, Houston, Texas, 1967.

Kavanagh, L. D., Jr., A revised ($B$, $L$) coordinate system to allow for the distention of the magnetosphere by a symmetric ring current, *J. Geophys. Res., 73,* 185, 1968.

Lazarus, A. J., H. S. Bridge, and J. Davis, Preliminary results from the Pioneer 6 MIT plasma experiment, *J. Geophys. Res., 71,* 3787, 1966.

Lees, L., Interaction between the solar plasma wind and the geomagnetic cavity, *Am. Inst. of Aeronautics and Astronautics, 2,* 1576, 1964.

Lüst, R., The properties of interplanetary space, in *Solar-Terrestrial Physics,* edited by J. W. King and W. S. Newman, p. 1, Academic Press, New York, 1967.

Mead, G. D., Deformation of the geomagnetic field by the solar wind, *J. Geophys. Res., 69,* 1181, 1964.

Mead, G. D., and D. B. Beard, Shape of the geomagnetic field solar wind boundary, *J. Geophys. Res., 72,* 2737, 1967.

Mead, G. D., and L. J. Cahill, Jr., Explorer 12 measurements of the distortion of the geomagnetic field by the solar wind, *J. Geophys. Res., 73,* 991, 1968.

Ness, N. F., C. S. Scearce, and J. B. Seek, Initial results of the IMP 1 magnetic field experiment, *J. Geophys. Res., 69,* 3531, 1964.

Patel, V. L., and A. J. Dessler, Geomagnetic activity and size of magnetospheric cavity, *J. Geophys. Res., 71,* 1940, 1966.

Schield, M. A., The configuration of geomagnetic field lines above the auroral zones, Ph.D. thesis, Rice University, Houston, Texas, 1968.

Sckopke, N., A general relation between the energy of trapped particles and the disturbance field near the earth, *J. Geophys. Res., 71,* 3125, 1966.

Sonnerup, B. U. Ö., and L. J. Cahill, Explorer 12 observations of the magnetopause current layer, *J. Geophys. Res., 73,* 1757, 1968.

Spreiter, J. R., A. L. Summers, and A. Y. Alksne, Hydromagnetic flow around the magnetosphere, *Planetary Space Sci., 14,* 223, 1966.

Wilcox, J. M., K. H. Schatten, and N. F. Ness, Influence of interplanetary magnetic field and plasma on geomagnetic activity during quiet-sun conditions, *J. Geophys. Res., 72,* 19, 1967.

Williams, D. J., and G. D. Mead, Nightside magnetosphere configuration as obtained from trapped electrons at 1100 kilometers, *J. Geophys. Res., 70,* 3017, 1965.

(Received June 27, 1968;
revised November 5, 1968.)